Goad, W. B., & Kanehisa, M. I. (1982) *Nucleic Acids Res. 10*, 247-263.
Grosveld, G. C., Shewmaker, C. K., Jat, P., & Flavell, R. (1981) *Cell (Cambridge, Mass.) 25*, 215-226.
Heintz, N. H., & Hamlin, J. L. (1982) *Proc. Natl. Acad. Sci. U.S.A. 78*, 6043-6047.
Hendrickson, S. L., Wu, J. R., & Johnson, L. F. (1980) *Proc. Natl. Acad. Sci. U.S.A. 77*, 5140-5144.
Henikoff, S., Keene, M. A., Fechtel, K., & Fristrom, J. W. (1986) *Cell (Cambridge, Mass.) 44*, 33-42.
Kaufman, R. J., & Sharp, P. A. (1983) *J. Mol. Biol. 159*, 601-621.
Lazowska, J., Jacq, C., & Slonimski, P. P. (1980) *Cell (Cambridge, Mass.) 22*, 333-348.
Levanon, D., Lieman-Hurwitz, J., Dafni, N., Wigderson, M., Sherman, L., Bernstein, Y., Laver-Rudich, Z., Danciger, E., Stein, O., & Groner, Y. (1985) *EMBO J. 4*, 77-84.
Leys, E. J., & Kellems, R. E. (1981) *Mol. Cell. Biol. 1*, 961-971.
Liu, L. F. (1983) *Crit. Rev. Biochem. 15*, 1-24.
Masters, J. N., & Attardi, G. (1985) *Mol. Cell. Biol. 5*, 493-500.
McGrogan, M., Simonsen, C. C., Smouse, D. T., Farnham, P. J., & Schimke, R. T. (1985) *J. Biol. Chem. 260*, 2307-2314.
McKnight, S. L., & Kingsbury, R. (1982) *Science (Washington, D.C.) 217*, 316-324.
McKnight, S. L., Kingsbury, R. C., Spence, A., & Smith, M. (1984) *Cell (Cambridge, Mass.) 37*, 253-262.
Melton, D. W., Konecki, D. S., Brennand, J., & Caskey, C. T. (1984) *Proc. Natl. Acad. Sci. U.S.A. 81*, 2147-2151.
Milbrandt, J. D., Heintz, N. H., White, W. C., Rothman, S., & Hamlin, J. L. (1981) *Proc. Natl. Acad. Sci. U.S.A. 79*, 4083-4087.
Milbrandt, J. D., Azizkhan, J. C., Greisen, K. S., & Hamlin, J. L. (1983) *Mol. Cell. Biol. 3*, 1266-1273.
Mitchell, P. J., Carothers, A. M., Han, J. H., Harding, J. D., Kas, E., Venolia, L., & Chasin, L. A. (1986) *Mol. Cell. Biol. 6*, 425-440.
Montoya-Zavala, M., & Hamlin, J. L. (1985) *Mol. Cell. Biol. 5*, 619-627.
Nunberg, J. H., Kaufman, R. J., Chang, A. C. Y., Cohen, S., & Schimke, R. T. (1980) *Cell (Cambridge, Mass.) 19*, 355-364.
Osborne, T. F., Goldstein, J. L., & Brown, M. S. (1985) *Cell (Cambridge, Mass.) 42*, 203-212.
Rigby, P. W. J., Dieckmann, M., Rhodes, C., & Berg, P. (1977) *J. Mol. Biol. 113*, 237-251.
Roebuck, K. A., & Stumph, W. E. (1985) *DNA 4*, 86-96.
Sanger, F., Nicklen, S., & Coulson, A. R. (1977) *Proc. Natl. Acad. Sci. U.S.A. 74*, 5463-5467.
Santiago, C., Collins, M., & Johnson, L. F. (1983) *J. Cell Physiol. 118*, 79-86.
Shimada, T., Inokuchi, K., & Nienhuis, A. W. (1986) *J. Biol. Chem. 261*, 1445-1452.
Staden, R. (1982) *Nucleic Acids Res. 10*, 2951-2961.
Valerio, D., Duyvesteyn, M. G. C., Dekkler, B. M. M., Weeda, G., Berkvens, T. M., van der Voorn, L., van Ormondt, H., & van der Eb, A. J. (1985) *EMBO J. 4*, 437-443.
Yanisch-Perron, C., Vieira, J., & Messing, J. (1985) *Gene 33*, 103-109.

Changes in Retinal Position during the Bacteriorhodopsin Photocycle: A Resonance Energy-Transfer Study†

C. A. Hasselbacher and T. G. Dewey*
Department of Chemistry, University of Denver, Denver, Colorado 80208
Received February 21, 1986; Revised Manuscript Received June 19, 1986

ABSTRACT: Distances from fluorescent lipid probes to the retinal chromophore of bacteriorhodopsin incorporated into asolectin vesicles have been measured with resonance energy transfer. Steady-state fluorescence is used to find the distance of closest approach from fluorescent lipid probes to ground-state retinal. Phase modulation of resonance energy transfer is used to find distances for retinal in bacteriorhodopsin's M intermediates. This latter technique uses an actinic light source to drive the photocycle while absorbance of a photocycle intermediate and fluorescence due to energy transfer to that intermediate are monitored with phase-sensitive detection. The photocycle intermediate concentration is varied by changing the frequency of modulation of the actinic light. Previous measurements of distances to the M intermediates using this technique [Hasselbacher, C. A., Preuss, D. K., & Dewey, T. G. (1986) *Biochemistry 25*, 668-676] are extended by use of several different fluorescent probes allowing labeling of either the bilayer surfaces or the interior. This provides a more detailed mapping of retinal's position. Analysis of the phase modulation data is improved in several ways to obtain accurate distances for the M intermediates. These distances are compared to ground-state distances. Results show that retinal is buried more deeply in the protein when bacteriorhodopsin is in its ground state than in either M state. There is also a significant change in retinal location between the slow-decaying and fast-decaying M intermediates. These large changes in retinal's position during the photocycle demonstrate the flexibility of monomeric bacteriorhodopsin.

Bacteriorhodopsin is a membrane-bound protein synthesized by the archaebacterium *Halobacterium halobium*. It actively transports protons across the bacterial membrane and maintains the proton gradient required for metabolic processes during oxygen deprivation. The proton pumping process is initiated by the absorption of light by bacteriorhodopsin's

† This research was supported in part by NSF Grant DMB-8315263.

0006-2960/86/0425-6236$01.50/0

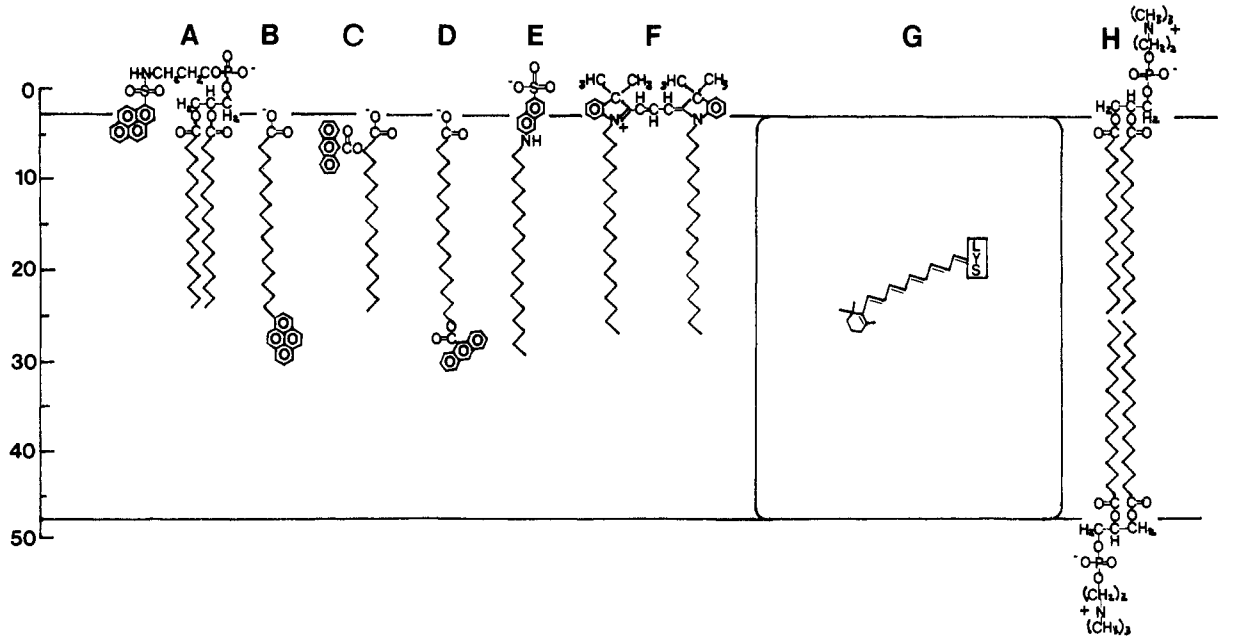

FIGURE 1: Schematic representation of structures and probable orientations of fluorescent lipid donors in the asolectin bilayer: (A) PyS-PE; (B) PyHA; (C) 2-AP; (D) 16-AP; (E) OANS; (F) DiI. A possible orientation of retinal in bR is also shown (G) (King & Schoenborn, 1982). The positions of the phospholipids of a dipalmitoylphosphatidylcholine bilayer (G) are included for comparison (distance between phosphate groups, 50.3 Å) (Stamatoff et al., 1979).

retinal chromophore. To elucidate the molecular mechanism of proton pumping, changes in the location and orientation of retinal during the photocycle must be determined. In this study, resonance energy transfer is used to determine the location of the retinal of bacteriorhodopsin in the ground state and in the M intermediate photocycle states. The distance of closest approach of fluorescent lipid donors at the surface or in the interior of the membrane to the retinal is determined.

A new phase modulation technique (Hasselbacher et al., 1986) is used to measure distances to the retinal in the M intermediate state. The utility of the phase modulation of resonance energy-transfer technique for measuring structural changes in photocycle states was demonstrated in our previous work. In this work we extend our measurements to a wider variety of probes. In these experiments the main source of error in the distances is due to assumptions made concerning the orientation of the transition dipoles of the donors and the acceptors. We provide a more detailed analysis of this assumption. In separate experiments, resonance energy transfer to the ground-state retinal was measured with conventional steady-state fluorescence. With fluorescent probes with spectral properties that permit energy transfer to both states, a direct comparison can be made of distances in the ground state and in the two M states. Our results show that the retinal is located in a significantly different position in each of these three states.

Materials and Methods

Chemicals. *N*-(1-Pyrenesulfonyl)dipalmitoyl-L-α-phosphatidylethanolamine (PyS-PE),[1] 1-pyrenehexadecanoic acid, 2-(9-anthroyloxy)palmitic acid, 16-(9-anthroyloxy)palmitic acid, 2-(*N*-octadecylamino)naphthalene-6-sulfonic acid, 1,1′-dioctadecyl-3,3,3′,3′-tetramethylindocarbocyanine perchlorate, and 1,6-diphenyl-1,3,5-hexatriene were purchased form Molecular Probes. Asolectin (soybean phospholipid) was obtained from Associated Concentrates. *N*-Octyl-β-D-glucopyranoside (octylglucoside) was from Sigma. Solvents were spectral grade and all chemicals were reagent grade. All solutions were made from distilled, deionized water.

Purple Membrane and Reconstituted Vesicles. H. halobium S-9 was grown in defined media (Lanyi & MacDonald, 1979). Purple membrane was purified with a sucrose step gradient (Becher & Cassim, 1975). Bacteriorhodopsin was reconstituted into asolectin vesicles with an octyl glucoside dilution technique (Racker et al., 1979), as previously modified (Hasselbacher et al., 1986). Vesicles have been characterized with respect to protein/lipid ratio and bR orientation. These previous results indicated that the vesicles in a given sample are uniformly distributed with respect to size and protein content and that the bR is oriented essentially 100% "inside out" relative to the in vivo orientation (Hasselbacher et al., 1986).

A variety of fluorescent labels were used to determine distances from defined locations in the lipid bilayer. These probes and their probable orientations in the bilayer are illustrated in Figure 1. For samples in which the probe labeled both the inner and outer vesicle surfaces, the probe was dissolved with asolectin in a suitable solvent and the solvent evaporated under nitrogen. The sample was then sonicated. For labeling of the outer vesicle surface only, the probe was dissolved in an organic solvent and added while stirring to the bR-reconstituted vesicles. Total added solvent never exceeded 1% of the total sample volume. Measurements were made when the probe fluorescence stabilized, indicating maximal dye was incorporated into the vesicles. This incorporation was always complete within 1 h. Cu^{2+} quenching of surface-labeled probe fluorescence was used as described previously to determine whether a given probe will readily migrate from the outer surface to the inner surface of the bilayer (Hasselbacher et al., 1986).

[1] Abbreviations: bR, bacteriorhodopsin; PyS-PE, *N*-(1-pyrenesulfonyl)dipalmitoyl-L-α-phosphatidylethanolamine; PyHA, 1-pyrenehexadecanoic acid; DiI, 1,1′-dioctadecyl-3,3,3′,3′-tetramethylindocarbocyanine perchlorate; 2-AP, 2-(9-anthroyloxy)palmitic acid; 16-AP, 16-(9-anthroyloxy)palmitic acid; DPH, 1,6-diphenyl-1,3,5-hexatriene; OANS, 2-(octadecylamino)naphthalene-6-sulfonic acid; Tricine, *N*-[tris(hydroxymethyl)methyl]glycine; EDTA, ethylenediaminetetraacetic acid; DPPC, dipalmitoylphosphatidylcholine.

Table I: Energy Transfer Parameters

fluorescent lipid probe	λ_{ex}	Q_D	$10^{13}J_{(gs)}$	$10^{14}J_{(M)}$	$\bar{r}$	$\langle d_D^x \rangle$	d	κ^2	$R_{0(gs)}$[a] (Å)	$R_{0(M)}$[b] (Å)	$R_{0(M)}$[c] (Å)
OANS[c]	308	0.20	1.14	8.9	0.135	0.581	22	0.884	39.3	39.5	37.7
OANS[d]							25	1.03	39.3	40.5	37.7
2-AP[c]	365	0.41	1.67	6.3	0.214	0.731	18	0.902	47.2	42.2	40.1
16-AP	365	0.55	1.58	6.2	0.101	0.503	0	0.573	49.1	41.0	42.0
Pys-PE[c]	353	0.47	1.22	7.7	0.058	0.379	21	0.661	45.8	42.4	42.5
PyHA	340	0.32	0.99	8.0	0.040	0.318	0	0.556	41.6	38.9	40.1
DPH	365	0.79									
DiI	540	0.21	4.12						48.9		
DiI[e]		0.12	4.18						44.8		

[a] Calculated with $\kappa^2 = {}^2/_3$. [b] Calculated with κ^2 values listed in the table. [c] Two vesicle surfaces labeled. [d] One vesicle surface labeled. [e] DPPC vesicles, 38 °C; from Hasselbacher et al. (1984).

For energy transfer to the ground state, the surface density of bR was varied by preparing samples with different protein to lipid ratios. For the M intermediate-state measurements, the surface density was varied by changing the frequency of modulation of the actinic light. In both cases the surface density was calculated by assuming a surface area of 875 Å^2 for a bR molecule (Henderson & Unwin, 1975) and a surface area of 68 Å^2 per lipid (Huang & Mason, 1978). With these values, the surface densities were determined as described previously (Hasselbacher et al., 1984, 1986). The bR concentration was obtained with an extinction coefficient of 62 700 M^{-1} cm^{-1} at 568 nm (Rehorek & Heyn, 1976). The M intermediate concentration was determined from the phase-modulated amplitudes of the absorbance signals by using the difference in the extinction coefficient between the M state and the ground state. A value of 36 000 M^{-1} cm^{-1} was used (Becher et al., 1978). The concentration of asolectin was determined by weight by assuming a molecular weight of 740 (Cerione et al., 1983).

Spectroscopic Measurements. Determination of Quantum Yield and Emission Anisotropy for Fluorescent Probes. Quantum yields for 2-AP, 16-AP, PyHA, OANS, DiI, and PyS-PE in asolectin vesicles were determined by the method of Chen (1967). DPH in cyclohexane was used as a standard with a quantum yield of 0.78 (Berlman, 1965). Absorbances were measured on a Varian Cary 219 spectrophotometer with all samples balanced against vesicle blanks to eliminate light scattering contributions. Corrected fluorescence spectra were obtained with a Spex Fluorolog 2 spectrofluorometer with an excitation bandwidth of 1.8 nm and an emission bandwidth of 2.25 nm. The measured quantum yields are presented in Table I. Wavelength-dependent polarization of fluorescent emission was measured with a Perkin-Elmer MPF-3L spectrophotometer equipped with Perkin-Elmer 063-0568 polarizers. The molar ratio of lipid to fluorophore was 200:1 in all these experiments. The emission anisotropy was corrected for instrument polarization (Chen & Bowman, 1965; Azumi & McGleen, 1962) and is given in Table I.

Distance Measurements. The distance of closest approach was measured from fluorescent lipid probes to the ground-state retinal by measuring the ratio of the steady-state fluorescence intensities of donors in vesicles in the presence and absence of bR. This ratio was determined over a range of protein surface densities and was analyzed with the theory of Wolber & Hudson (1979). Reported distances represent an average of the points at all surface densities. For 2-AP and 16-AP, the excitation wavelength was 365 nm and 100 × 1 s readings of the fluorescent emission at 459 nm were averaged. In separate experiments, DiI quenching was observed from the outer vesicle surface and from both surfaces. The DiI excitation wavelength was 540 nm and the emission was monitored at 575 nm. Occasionally, DiI samples showed excimer peaks. These were not included in our measurements.

Energy transfer to the M intermediate states was measured with the phase–lifetime spectrometer described previously (Hasselbacher et al., 1986). The M intermediate was monitored by the absorbance at 402 nm. The degree of quenching due to resonance energy transfer was determined from the modulated fluorescent amplitudes. The fluorescent excitation wavelengths were 365 nm for 2-AP and 16-AP, 353 nm for PyS-PE, 340 nm for PyHA, and 308 nm for OANS. The spectral bandwidth of the probe beam was 8 nm. The measured absorbances in the phase–lifetime spectrophotometer were normalized to those measured on a Varian Cary 219 by using Ditric neutral density filters as standards. Fluorescence signals were corrected for inner filter effects due to the modulated absorption of the excitation light by the photocycle. This correction was calculated by making use of previously derived equations (Brand & Wiltholt, 1967)

$$\Delta F_{IF} = F_0[2.303(A + \Delta A)/(1 - 10^{-(A+\Delta A)}) - 2.303A/(1 - 10^{-A})] \quad (1)$$

where ΔF_{IF} is the modulated fluorescence due to inner filter effects, F_0 is the total fluorescence (DC signal) observed, A is the total absorbance at the excitation wavelength, and ΔA is the modulated absorbance at the excitation wavelength. ΔF_{IF} is then subtracted from the observed, modulated fluorescent signal. This correction was made at each frequency of the modulated actinic light.

The characteristic Foerster distance, R_0, for each of the donor–acceptor pairs used was determined with eq 2, where n is the refractive index of the medium, κ^2 is a geometric factor

$$R_0 = (9.79 \times 10^3 \text{ Å})(J\kappa^2 Q_D n^{-4})^{1/6} \quad (2)$$

characterizing the relative orientations of the transition dipoles of the donor and acceptor, Q_D is the quantum yield of the donor, and J is an overlap integral determined from the donor's emission and acceptor's absorbance spectra. The values of J determined for both the retinal ground-state acceptor and the M intermediate-state acceptor are given in Table I. For these determinations the absorbance spectra of monomeric, ground-state bR in asolectin vesicles were measured. These were compared to results with DMPC vesicles when bR is aggregated (10 °C) and monomeric (30 °C). Above the phase transition the absorbance shows little temperature dependence. The maximum of the monomeric absorbance spectrum is shifted to lower wavelengths compared to the aggregate spectrum. It has an absorbance maximum at 550 nm with an extinction coefficient of 58 000 M^{-1} cm^{-1}. The retinal absorbance spectrum for the M intermediate obtained previously (Becher et al., 1978) was used for J determinations for the photocycle state. The refractive index was taken to be that of hexane, which is 1.38 (*CRC Handbook of Chemistry*

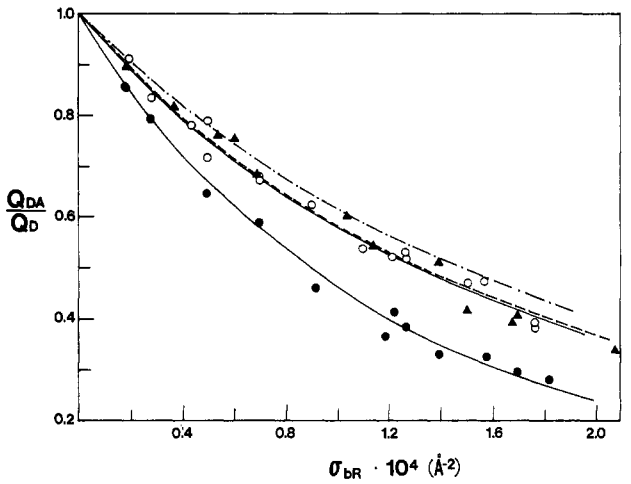

FIGURE 2: Quenching of lipid probe fluorescence by bR incorporated into asolectin vesicles. Fluorescence in the presence of retinal acceptor divided by fluorescence in the absence of acceptor (Q_{DA}/Q_D) is plotted vs. surface density of acceptor, (σ_{bR}). Fluorescent probes used are 16-AP (●), 2-AP labeling both vesicle surfaces (○), and DiI labeling outer vesicle surface (▲). Theoretical curves (solid lines for 16-AP and 2-AP and dashed line for DiI) are obtained with the theory of Wolber and Hudson (1979) and average values for L. The curve representing quenching of DiI fluorescence for DiI labeling both vesicle surfaces (–·–) is shown for comparison (Hasselbacher et al., 1985).

and Physics, 1981). This value was used because energy transfer occurs predominantly through the lipid membrane in these experiments. R_0 is not a sensitive function of the refractive index and using the water value of 1.33 results in a 1% difference in the distances measured. The major source of error is due to uncertainties in the orientation factor. All other parameters may be determined or estimated, giving an accuracy in the distance measurement of approximately 1%. The value of κ^2 was taken to be $^2/_3$, which corresponds to the case of rapid rotational averaging of the donor and acceptor orientations. The error inherent in this assumption is analyzed in detail in the following section for energy transfer to the M state.

RESULTS

In this work the efficiency of resonance energy transfer is measured between donors and acceptors located in different planes. The complicated situation of multiple donors and multiple acceptors in two dimensions has been analyzed by a number of theoretical approaches (Shaklai et al., 1977; Estep & Thompson, 1979; Wolber & Hudson, 1979; Dewey & Hammes, 1980; Snyder & Friere, 1982). Resonance energy transfer to ground-state bR was analyzed with the approach to Wolber and Hudson (1979). Quenching of fluorescence vs. surface density of bR is shown in Figure 2 for fluorescent probe in the center of the bilayer (16-AP), on both bilayer surfaces (2-AP), and on one bilayer surface (DiI). Because asolectin is above its phase transition temperature in these experiments (22 °C), bR is monomeric. The dashed line in Figure 2 represents quenching of DiI fluorescence by monomeric bR when both membrane surfaces are labeled in DPPC vesicles at 38 °C (Hasselbacher et al., 1984). DiI labeled on the outer surface showed no significant internalization after 24 h. It has been previously established that the time constant for transfer of DiI from one side of the membrane to the other is comparable to that of phospholipids and is quite slow (Fahey & Webb, 1978). Therefore, this probe allowed the measurement of the distance from the outer vesicle surface to the ground-state retinal. In contrast, 2-AP equilibrated rapidly between the bilayer surfaces as indicated by

Table II: Distances from Fluorescent Lipid Probes to Retinal

distance measd	fluorescent lipid probe	L (Å) (calcd κ^2)	L (Å) ($\kappa^2 = ^2/_3$)
to ground-state retinal	2-AP[a]		29.0 ± 3.3[d]
	16-AP		17.7 ± 3.2
	DiI[b]		32.0 ± 2.8
	DiI[a,c]		28.0 ± 1.0
to slow-decaying M intermediate	PyHA	14.9 ± 0.2	15.6 ± 0.2
	16-AP	13.2 ± 0.1	13.8 ± 0.1
2-AP[a]	23.1 ± 1.9	21.4 ± 1.8	23.6 ± 0.6
	OANS[b]	27.3 ± 0.2	24.7 ± 0.1
	OANS[a]	23.3 ± 0.3	21.8 ± 0.3
to fast-decaying M intermediate	PyHA	15.7 ± 1.0	16.4 ± 1.0
	16-AP	13.3 ± 0.7	13.9 ± 0.6
	2-AP[a]	24.9 ± 7.0	23.1 ± 6.4
	PyS-PE[a]	26.3 ± 4.8	26.4 ± 4.9
	OANS[b]	27.1 ± 0.2	24.4 ± 0.3
	OANS[a]	25.6 ± 2.8	23.8 ± 2.5

[a] Both vesicle surfaces labeled with fluorescent probe. Distances represent a sum of contributions in accord with eq 19. [b] Outer vesicle surface only labeled with fluorescent probe. [c] DPPC vesicles, 38 °C; from Hasselbacher et al. (1984). [d] Error for ground-state values is standard deviation of data points. Error for M intermediate values calculated from standard deviation of m_1 and m_2.

Cu^{2+} quenching. Values of the distance of closest approach, L, are shown in Table II for all of the donors.

The M intermediate experiments provide a simpler situation because of the extremely low surface density of acceptor. In the reconstituted system there are approximately 100 bR molecules per vesicle. During the phase modulation experiment approximately 0.1% of the bR populates the M state. It is therefore unlikely that a significant number of vesicles simultaneously contain two M state proteins. It is also unlikely that significant energy transfer occurs between vesicles. This is due to the extremely low concentration of vesicles in the samples. This concentration is estimated to be on the order of 10 nM. The resulting average distance between vesicles is too large for significant energy transfer. Therefore, the M intermediate experiments represents a situation where multiple donors transfer energy to a single acceptor. The efficiency of energy transfer, E, is related to a sum over the N donors that involves the distances of separation of the ith donor from the acceptor, R_i (Sklar et al., 1977; Haigh et al., 1979)

$$E/(1 - E) = Q_{DA}/Q_D = \sum_{i=1}^{N} (R_0/R_i)^6 \quad (3)$$

where Q_{DA} and Q_D are the quantum yield of the donor in the presence and absence of acceptor, respectively, and are experimentally measured parameters. With the assumption of a uniform distribution of identical donors, the summation may be converted to an integral. This gives

$$E/(1 - E) = P_V \int_L^\infty (R_0/R)^6 \, dP = \sigma_A \pi R_0^6/4L^4 \quad (4)$$

where P_V is the probability of finding an acceptor in a given vesicle and is given by n_A/n_V, the ratio of the number of acceptors to the number of vesicles. P is the probability of finding the donor–acceptor pair separated by a distance R on a given vesicle and $dP = 2\pi R \, dR/S_V$, where S_V is the surface area of a vesicle. σ_A is the surface density of acceptor. L is the distance of closest approach of a donor to an acceptor.

The major error that occurs in measuring distances by resonance energy transfer is due to uncertainties in the orientation factor, κ^2. Because of this, an extensive literature has developed for estimating limits on this value from fluorescence emission anisotropies (cf., Dale et al., 1979). In most work on membrane systems, κ^2 has been assumed to equal $^2/_3$. This is the correct value when the donor's and acceptor's orienta-

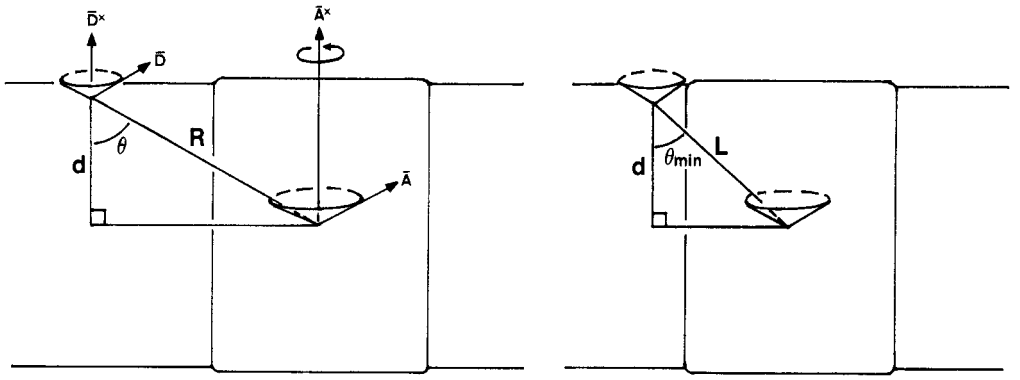

FIGURE 3: Schematic of relationship between donor emission transition moment (D) and acceptor absorbance transition moment (A) used for κ^2 calculations presented in the text. κ^2 is a function of θ for donors and acceptors in separated planes (Davenport et al., 1985). Donors are fluorescent lipid probes; acceptor is retinal in one of the M intermediates of bacteriorhodopsin. d is the difference in position between donor and acceptor along a line perpendicular to the membrane. R is the separation distance between donor and acceptor, which becomes a minimum distance at L, the distance of closest approach. Rotation of chromophores occurs about the projections of the donor emission and acceptor absorbance transition moments, D^x and A^x, respectively. Rotation of the acceptor, retinal, is shown in the text to be restricted to rotation of the entire protein.

tions are dynamically averaged during the fluorescent lifetime of the donor. A detailed error anaysis of the orientation factor for membrane systems has recently been presented (Davenport et al, 1985). Our experiments involving the M intermediate provide a simpler situation because it represents energy transfer from multiple donors to a single acceptor. We have adapted the analysis of Davenport et al. (1985) to this case and obtain exact analytic expressions. These expressions allow one to accurately account for orientation effects provided the emission anisotropy of the donor and acceptor are known. Because the M intermediate state is not fluorescence, this information could not be obtained directly for the acceptor. Instead we estimate the M state retinal emission anisotropy by using the extreme case of the retinal being immobilized in the protein. This provides a limiting value for κ^2 and allows an estimate of the error in the distance measurement.

Figure 3 shows the donor–acceptor geometry that is considered for the κ^2 analysis. The positions of donor emission and acceptor absorbance transition moments are oriented with radial symmetry about axes parallel to the bilayer normal and are dynamically averaged. The orientation factor is a function of the angle, θ, formed between the membrane normal and the line joining the donor and acceptor in the transverse plane of the membrane. For this donor–acceptor distribution, κ^2 is expressed as (Davenport et al., 1985)

$$\kappa^2(\theta) = (1 - 3\cos\theta)\langle d_D^x\rangle\langle d_A^x\rangle + \tfrac{1}{3}(1 - \langle d_D^x\rangle) + \tfrac{1}{3}(1 - \langle d_A^x\rangle) + \cos\theta\langle d_D^x\rangle(1 - \langle d_A^x\rangle) + \langle d_A^x\rangle(1 - \langle d_D^x\rangle) \quad (5)$$

The axial depolarization factors for donor and acceptor are $\langle d_D^x\rangle$ and $\langle d_A^x\rangle$, respectively. The axial depolarization factor for the donor was calculated from the experimentally determined emission anisotropy value, r_∞, using

$$\langle d_D^x\rangle = (r_\infty/0.4)^{1/2} \quad (6)$$

Because $\langle d_A^x\rangle$ could not be determined, it was estimated for a limiting case. The extreme case is considered in which the M state retinal is immobilized in the protein as in the case for ground-state retinal (Kouyama et al., 1985; Razi Naqvi et al., 1973; Sherman et al., 1976; Korenstein & Hess, 1978). In this situation the major contribution to the rotational anisotropy of the chromophore is due to the rotation of the entire protein in the membrane. Time-resolved absorption anisotropy measurements of rotation of bR monomers (Cherry et al., 1977) show a decay from a limiting initial value above 0.1 to a value of 0.037 in less then 0.5 ms. Because the M intermediate lifetimes are much longer than this decay, the retinal orientation is averaged by rotation of the entire protein. The situation where rotation of the entire macromolecule is included in the orientation factor has been analyzed by Strittmater and co-workers (Koppel et al., 1979). With this analysis, $\langle d_A^x\rangle$ was calculated by

$$\langle d_A^x\rangle = \tfrac{3}{2}\overline{\langle\cos^2\theta_A\rangle} - \tfrac{1}{2} \quad (7)$$

where

$$\overline{\langle\cos^2\theta_A\rangle} = \tfrac{1}{2}\overline{(\sin^2\theta_{A'}\langle\sin^2\theta_{A''}\rangle)} + \overline{(\cos^2\theta_{A'}\langle\cos^2\theta_{A''}\rangle)} \quad (8)$$

$\overline{\cos^2\theta_{A'}}$, characterizing reorientations of the chromophore relative to the macromolecule, was determined with (Fleming et al., 1979)

$$\cos^2\theta_{A'} = [1 + 2(EA/0.4)^{1/2}]/3 \quad (9)$$

where EA is the absorbance anisotropy of bR in the purple membrane. EA has a value of 0.395 ± 0.005 (Kouyama et al., 1981). The fundamental emission anisotropy is 0.4. In the same manner, $\cos^2\theta_{A''}$, characterizing rotation of the entire macromolecule in the bilayer, is expressed as

$$\cos^2\theta_{A''} = [1 + 2(0.037/0.4)^{1/2}]/3 \quad (10)$$

using the absorbance anisotropy value of 0.037 (Cherry et al., 1977). From eq 8, $\langle d_A^x\rangle$ was determined to be 0.312.

The effect of the θ dependence of κ^2 on the energy-transfer efficiency was determined by substituting eq 5 into the expression for R_0 (eq 2). With the relationship $d/R = \cos\theta$, the angular dependence is converted into a radial dependence. This was then included in the calculation of the energy-transfer efficiency using

$$E/(1 - E) = 2\pi\sigma_A\int_L^\infty (R_0^6/R^6)R\,dR \quad (11)$$

Integration then yields

$$E/(1 - E) = 2\pi\sigma_A(R_0')^6[(d^2(\langle d_D^x\rangle(1 - \langle d_A^x\rangle) + \langle d_A^x\rangle \times (1 - \langle d_D^x\rangle) - 6\langle d_D^x\rangle\langle d_A^x\rangle))]/6L^6 + (2 - \langle d_D^x\rangle - \langle d_A^x\rangle + 3\langle d_D^x\rangle\langle d_A^x\rangle)/12L^4 + (9\langle d_D^x\rangle\langle d_A^x\rangle d^4)/8L^8] \quad (12)$$

where

$$(R_0')^6(\kappa^2) = R_0^6 \quad (13)$$

The vertical distance between donor and acceptor in the bilayer, d, is estimated with Figure 1. In this figure, the fluorescent lipid probes used in these experiments are drawn to scale in their most probable membrane locations (see Discussion). Because the two terms of eq 12 in which d

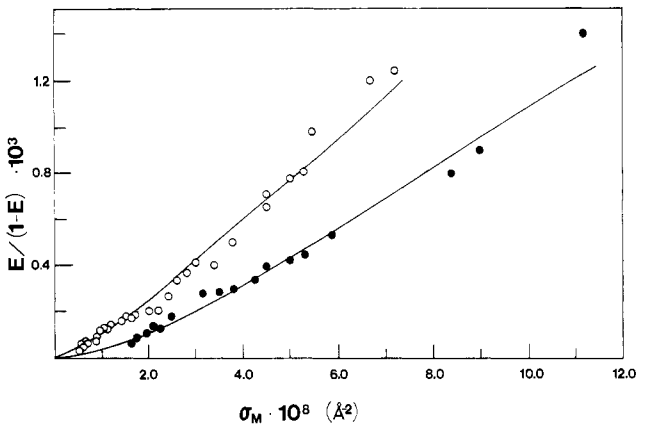

FIGURE 4: Plot of efficiency of energy transfer from surface-labeling fluorescent lipid probes, Pys-PE (○) and 2-AP (●), to the M intermediates vs M intermediate surface density in asolectin vesicles. The fitted curves were obtained from bilinear regression, eq 25.

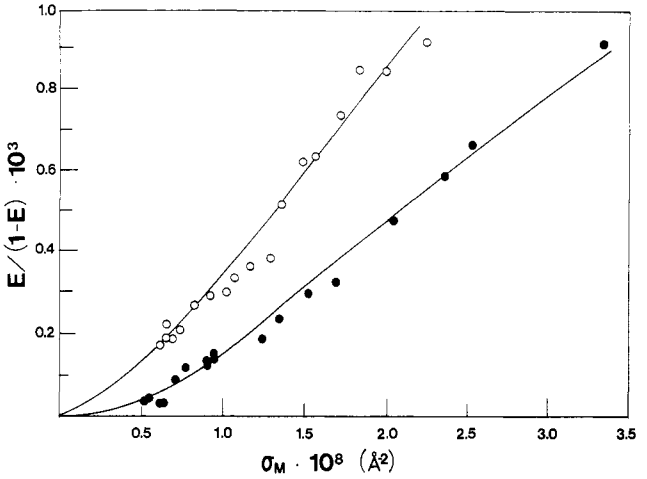

FIGURE 5: Plot of efficiency of energy transfer from fluorescent probes labeling the bilayer interior, PyHa (○) and 16-AP (●), to the M intermediates vs. M intermediate surface density in asolectin vesicles. The fitted curves were obtained as in Figure 4.

appears have opposite signs when all values of donor and acceptor axial depolarization factors are used, the results are not very sensitive to the particular values of d chosen. For fluorescent probes in the bilayer center (16-AP, PyHA), a change in d from 0 to 5 Å results in a change in L of less than 1%. Values of d used in these calculations are shown in Table I. With eq 12, the distance of closest approach is determined. κ^2 values were calculated with these distances and eq 4. Calculated values for κ^2 are listed in Table I. Characteristic Foerster distances obtained with these calculated κ^2 values are compared in Table I to those obtained by assuming rapid relative rotation of donor and acceptor ($\kappa^2 = {}^2/_3$). The change in R_0, on the average, is less than 4% when rapid rotation is assumed.

Efficiencies of energy transfer vs. total M intermediate surface density are shown in Figures 4 and 5 for fluorescent probes labeling the membrane surface and interior, respectively. These plots are clearly nonlinear, indicating that the two M intermediates have different locations. Distances from fluorescent donors to the two M intermediates were determined by a bilinear fit (Hasselbacher et al., 1986)

$$E(\omega)/(1 - E(\omega)) = m_s\sigma_{M,s}(\omega) + m_f\sigma_{M,f}(\omega) \quad (14)$$

assuming $\kappa^2 = {}^2/_3$, $m_s = \pi R_0{}^6(2L_s{}^4)^{-1}$, and $m_f = \pi(R_0)^6(2L_f{}^4)^{-1}$. $\sigma_{M,s}$ and $\sigma_{M,f}$ are surface densities of the slow- and fast-decaying M intermediates respectively. Surface densities for each intermediate were calculated with fitted decay lifetimes and surface density amplitudes obtained from the nonlinear least-squares fit of the absorbance data as described below. The calculated surface densities were then used in a bilinear least-squares fit of eq 14 to obtain slopes m_s and m_f. The distances, L_s and L_f, calculated from these slopes are shown in Table II for $\kappa^2 = {}^2/_3$ or using the κ^2 analysis in eq 12.

In order to determine the extent of resonance energy transfer to each M intermediate, it is necessary to know the surface density for each intermediate. This may be determined from an analysis of the absorbance amplitude dispersion curve. The chopped actinic light represents a periodic square-wave driving force for the photocycle. The amplitude response, $A(\omega)$, for such a driving force is given by (Hasselbacher et al., 1986)

$$A(\omega) = \sum_i A_i \tanh(\pi/2\omega\tau_i) \quad (15)$$

where τ_i is the relaxation time of the ith mode, ω is the chopping frequency, and A_i is the amplitude of the ith relaxation process. An ideal amplifier would respond according to eq 15. Unfortunately, most amplifiers do not respond equally over the entire harmonic range. An analysis has been performed that corrects the response function, $A(\omega)$, for the harmonic sensitivity of the amplifier (T. G. Dewey, unpublished results). This Fourier analysis gives

$$A(\omega) = \sum_n\sum_i [H(n)A_i \sin(n((\pi/2) + \phi_{1i}) - \phi_{ni})]/[n(1 + n^2\omega^2\tau_i{}^2)^{1/2}] \quad (16)$$

where $H(n)$ is a function that describes the harmonic sensitivity of the amplifier, and $\tan\phi_{ni} = n\omega\tau_i$. For our amplifier, the PAR 5204, n is always odd and $H(n) = 1/n$. The absorbance amplitude dispersion curves were analyzed with a nonlinear least-squares fit to eq 16. In order to fit the data, i must equal 2. This is consistent with the two M intermediate states seen by most works using either phase or flash techniques. The summation in eq 16 was truncated at $n = 50$. Terms beyond this harmonic contribute less than 0.1% over the frequency range of our measured amplitudes. This analysis gives results that are similar to our previous analysis, which used eq 15 (Hasselbacher et al., 1986). The major difference is that our fitted amplitudes show the fast intermediate making less of a contribution to the overall amplitude. The amplitude ratios with this new analysis are now in agreement with those observed by Krupinsky and Hammes (1986) for a similar reconstituted system. Typical values for bR in asolectin vesicles are $\tau_1 = 54.9$ ms, $\tau_2 = 2.1$ ms, and $A_2/(A_1 + A_2) = 0.048$.

A correction was introduced to account for resonance energy transfer to ground-state bR. This energy transfer will be detected with the phase–lifetime spectrometer because the signal will be modulated due to ground-state bR depletion during the photocycle. Thus

$$E/(1 - E) = (R^6_{0(M)}\pi\sigma_M)/4L_M{}^4 + (R^6_{0(gs)}\pi\sigma_{(gs)})/4L^4_{(gs)} = (R^6_{0(M)}\pi\sigma_M)/4L^4_{obsd} \quad (17)$$

Assuming σ_M, the modulated M intermediate surface density, is equal to $-\sigma_{(gs)}$ gives

$$1/L^4_M = 1/L^4_{obsd} + [R_{0,bR}/R_{0,M}]^6(1/L^4_{bR}) \quad (18)$$

The distance of closest approach to the M intermediates was found from the observed L values by using eq 18. L_{bR} is the experimentally determined distance from ground-state retinal to 16-AP (for distances to the center of the bilayer), 2-AP (for distances to both bilayer surfaces), and DiI (for distances to the outer surface only) shown in Table II. Values of L for the M intermediates appearing in Table II are corrected with eq 18.

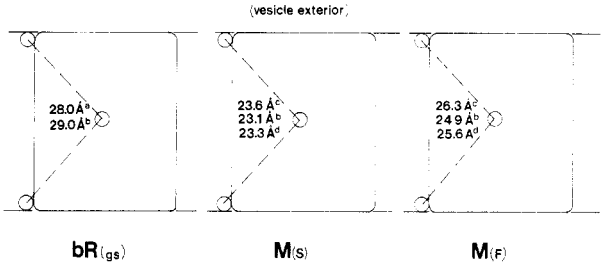

FIGURE 6: Schematic representation of distances found from retinal to fluorescent lipid probes labeling both bilayer surfaces for bacteriorhodopsin in the ground state (bR_{gs}), slow-decaying M intermediate (M_S), and fast-decaying M intermediate (M_F). Distances are measured from (a) DiI, (b) 2-AP, (c) PyS-PE, (d) OANS. Distances represent a sum of contributions as given by eq 19. Distances shown are not to scale.

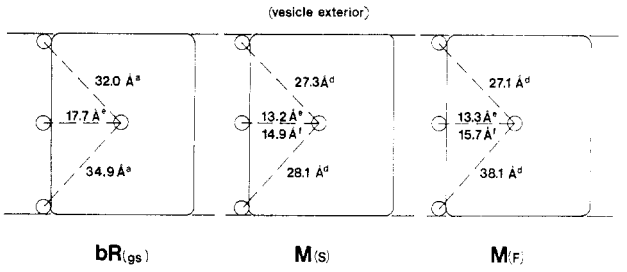

FIGURE 7: Schematic representation of distances found from retinal to fluorescent lipid probes labeling one bilayer surface or the bilayer interior for bacteriorhodopsin in the ground state (bR_{gs}), the slow-cycling M intermediate (M_S), and the fast-cycling M intermediate. Distances are measured from (a) DiI, (d) OANS, (e) 16-AP, and (f) PyHA. Distances shown are not to scale.

The distance from the inner bilayer surface to retinal was calculated from distances measured from both bilayer surfaces and from the outer bilayer surface using eq 19 (Hasselbacher et al., 1986)

$$L^{-4}\text{ (two surfaces)} = L^{-4}\text{ (outer surface)} + L^{-4}\text{ (inner surface)} \quad (19)$$

These distances are displayed in Figure 7 for ground-state retinal and for the slow- and fast-decaying M intermediates.

Discussion

Fluorescent membrane probes were used to determine distances from fixed locations in the lipid bilayer to retinal in the ground state and the M intermediate states of bacteriorhodopsin. To interpret the distances measured in this work, the position of the fluorescent lipid probes in the bilayer must be established. The *n*-(9-anthroyloxy) fatty acids have been characterized with respect to transverse location of the chromophore in the membrane using nuclear magnetic resonance and fluorescence quenching techniques (Podo & Blasie, 1977; Thulborn & Sawyer, 1978; Haigh et al., 1979). Haigh and co-workers investigated a series of *n*-(9-anthroyloxy) fatty acids (n = 2, 6, 7, and 12) by resonance energy transfer. Their results indicated that 2-AP is situated approximately 2 Å from the lipid–water interface. Extension of the distances found for these probes to the case of 16-AP yields a distance of 21 Å from the bilayer surface. Location of this probe near the center of the bilayer has also been established with fluorescence polarization (Frehland et al., 1982). The location of pyrenebutyric and pyrenedecanoic acid in DPPC vesicles has been established with fluorescence quenching (Kano et al., 1980; Correll et al., 1978). These probes orient in membranes with the carboxylate group near the hydrophilic surface and the chromophore buried in the hydrophobic interior. These results would suggest that PyHA will also be located near the center of the membrane. The chromophore of PyS-PE is considered to be near the lipid–water interface (Waggoner & Stryer, 1970). Kido and co-workers (1980) suggest that the PyS-PE chromophore is located in a more hydrophilic region of the lipid–water interface than the glycerol moiety of the phospholipids. Because the size, shape, and amphipathic character of DiI closely resembles that of phospholipids, the polar, fluorescent head group of this probe is located near the lipid–water interface (Fahey & Webb. 1978). The charged sulfonate group on OANS would most likely cause the chromophore to reside at the lipid–water interface. The probable positions of these fluorescent donors in the lipid bilayer are illustrated in Figure 1. The positions of DPPC molecules in a 50-Å membrane (Stamatoff et al., 1979) are included for comparison.

The distances measured with the various fluorescent probes are given in the schematic illustrations of Figures 6 and 7. These results are presented in tabular form in Table II. The spectral overlap of the anthroyloxy probes' fluorescent emission with the absorbance of the retinal of bR in both the M state and the ground state made it possible to measure a set of distances with a single probe. Thus, ambiquities due to comparing probes of different size and shape are avoided. The drawback of using such probes is that measurement of the resonance energy transfer to the M states will also reflect the loss of transfer efficiency due to depletion of the ground state. However, if the ground-state distance is determined independently as is done in this work, this effect can be corrected in a straightforward fashion with eq 18. Distances to the M intermediates were determined with the limiting value for κ^2 calculated from eq 12. These distances were compared (Table II) with those obtained by assuming rapid rotational averaging ($\kappa^2 = {}^2/_3$). Distances obtained in the M states using the limiting, calculated κ^2 values appear more consistent when comparing different probes. However, for all probes the difference in distances measured with the limiting value or the ${}^2/_3$ value for κ^2 is small. This indicates that the error in the measured distances due to uncertainty in κ^2 is at most 5%. This detailed analysis could not be used in the case of resonance energy transfer to the ground-state retinal because of the high surface densities used in those experiments. Nevertheless, given the emission anistropies of the probes, an uncertainty of 10% would be expected in these experiments based on previous theoretical results (Dale et al., 1979).

The magnitudes of these distance changes indicate that bacteriorhodopsin undergoes a significant structural change during its photocycle. Measurements with DI and 16-AP indicate that retinal in ground-state bR is located approximately halfway through a bilayer and in the radial center of the protein (effective monomer radius, 17 Å (Henderson & Unwin, 1975)). The measurements to the slow-decaying intermediate indicate that the retinal in this state is also near the bilayer center but is radially shifted closer to the periphery of the protein. This 3–5-Å change could be the result of either retinal configurational or apoprotein conformational changes. Retinal in the fast-decaying intermediate does not appear to be positioned symmetrically in the protein. The distance from the inner bilayer surface is significantly greater than that from the outer bilayer surface. Results from the labeling of both surfaces are consistent with these changes in position but tend not to be as dramatic. This is because the average distance from both surfaces is not as sensitive a parameter as the distance from one surface. The measured distances are shown in Figures 6 and 7 on an idealized, cylindrical model of bacteriorhodopsin. This model is not meant to represent the true

situation but rather serves as a schematic to display the data.

These results reveal the dynamic nature of bacteriorhodopsin structure during the photocycle. Since the M intermediates are formed on a relatively slow time scale, the protein has time to react to the electronic charge distribution of the retinal in the M state. Conformational adjustments can be made on this time scale that could minimize the energy of the retinal–protein interaction. In this view, the protein can be seen as "relaxing" into the most stable conformation in order to accommodate the retinal. This process may not occur with the fast photocycle intermediates because protein conformational processes may be too slow to react during the lifetime of the intermediate. Future work will concentrate on measurements of distances to the retinal in halorhodopsin. This retinal–protein has a quite different function than bacteriorhodopsin. The conformational dynamics of halorhodopsin's photocycle will offer a valueable comparison to the present results on bacteriorhodopsin.

Registry No. Retinal, 116-31-4.

REFERENCES

Azumi, T., & McGlynn, S. P. (1962) *J. Chem. Phys. 37*, 2413–2420.

Becher, B. M., & Cassim, J. Y. (1975) *Prep. Biochem. 5*, 161–178.

Becher, B. M., Tokunaga, F., & Ebrey, T. G. (1978) *Biochemistry 17*, 2293–2300.

Berlman, I. B. (1965) *Handbook of Fluorescence Spectra of Aromatic Molecules*, p 179, Academic, New York.

Brand, L., & Wiltholt, B. (1967) *Methods Enzymol. 11*, 776–855.

Cerione, R. A., McCarty, R. E., & Hammes, G. G. (1983) *Biochemistry 22*, 769–776.

Chen, R. (1967) *Anal. Biochem. 19*, 374–387.

Chen, R. F., & Bowman, R. L. (1965) *Science (Washington, D.C.) 147*, 729–731.

Cherry, R. J., Mueller, U., & Scheider, G. (1977) *FEBS Lett. 80*, 465–468.

Correll, G. D., Cheser, R. N., III, Nome, F., & Fendler, J. H. (1978) *J. Am. Chem. Soc. 100*, 1254–1262.

CRC Handbook of Chemistry and Physics (1978–1979) Vol. 59, p C-333, CRC Press, Boca Raton, FL.

Dale, R. E., Eisinger, J., & Blumberg, W. E. (1979) *Biophys. J. 26*, 161–194.

Davenport, L., Dale, R. E., Bisby, R. H., & Cundall, R. B. (1985) *Biochemistry 24*, 4097–4108.

Dewey, T. G., & Hammes, G. G. (1980) *Biophys. J. 32*, 1023–1035.

Estep, T. N., & Thompson, T. E. (1979) *Biophys. J. 26*, 195–207.

Fahey, P. F., & Webb, W. W. (1978) *Biochemistry 17*, 3046–3053.

Fleming, P. J., Koppel, D. E., Lau, A. L., & Strittmatter, P. (1979) *Biochemistry 18*, 5458–5464.

Frehand, E., Kreikenbohm, R., & Pohl, W. G. (1982) *Biophys. Chem. 15*, 73–86.

Haigh, E. A., Thulborn, K. R., & Sawyer, W. H. (1979) *Biochemistry 18*, 3525–3532.

Hasselbacher, C. A., Street, T. L., & Dewey, T. G. (1984) *Biochemistry 23*, 6445–6452.

Hasselbacher, C. A., Preuss, D. K., & Dewey, T. G. (1986) *Biochemistry 25*, 668–676.

Henderson, R., & Unwin, P. N. T. (1975) *Nature (London) 257*, 28–32.

Huang, C., & Mason, J. (1978) *Proc. Natl. Acad. Sci. U.S.A. 75*, 308–310.

Kano, K., Kawazumi, H., & Ogawa, T. (1980) *Chem. Phys. Lett. 74*, 511–515.

Kido, N., Tanaka, F., Kaneda, N., & Yagi, K. (1980) *Biochim. Biophys. Acta 603*, 255–265.

King, G. I., & Schoenborn, B. P. (1982) *Methods Enzymol. 11*, 241–248.

Koppel, D. E., Fleming, P. J., & Strittmatter, P. (1979) *Biochemistry 18*, 5450–5457.

Korenstein, R., & Hess, B. (1978) *FEBS Lett. 89*, 15–20.

Kouyama, T., Kinosita, K., & Ikegami, A. (1985) *Biophys. J. 47*, 43–54.

Krupinski, J., & Hammes, G. G. (1985) *Biochemistry 24*, 6963–6972.

Lanyi, J. K., & MacDonald, R. E. (1979) *Methods Enzymol. 56*, 398–407.

Podo, F., & Blasie, J. K. (1977) *Proc. Natl. Acad. Sci. U.S.A. 74*, 1032–1036.

Racker, E., Violand, B., O'Neal, S., Alfonzo, M., & Telford, J. (1979) *Arch. Biochem. Biophys. 198*, 470–477.

Razi Naqvi, K., Rodriguez, J. G., Cherry, R. J., & Chapman, D. (1973) *Nature (London), New Biol. 245*, 249–251.

Rehorek, M., & Heyn, M. P. (1979) *Biochemistry 18*, 4977–4983.

Shaklai, N., Yquerabide, J., & Ranney, H. M. (1977) *Biochemistry 16*, 5585–5592.

Sherman, W. V., Slifkin, M. A., & Caplan, S. R. (1976) *Biochim. Biophys. Acta 423*, 238–248.

Sklar, L. A., Hudson, B. S., & Ranney, H. M. (1977) *Biochemistry 16*, 5100–5108.

Snyder, B., & Friere, E. (1982) *Biophys. J. 40*, 137–148.

Stamatoff, J., Bilash, T., Ching, Y., & Eisenberger, P. (1979) *Biophys. J. 28*, 413–422.

Thulborn, K. R., & Sawyer, W. H. (1978) *Biochim. Biophys. Acta 511*, 125–140.

Waggoner, A. S., & Stryer, L. (1970) *Proc. Natl. Acad. Sci. U.S.A. 67*, 579–589.

Wolber, P. K., & Hudson, B. S. (1979) *Biophys. J. 28*, 197–210.